Morphology and transport properties of nanostructural gold on silicon

S. Pal, M. K. Sanyal,[a] S. Hazra, and S. Kundu
Surface Physics Division, Saha Institute of Nuclear Physics, 1/AF Bidhannagar, Kolkata 700 064, India

F. Schreiber[b]
Max-Planck-Institut für Metallforschung, Heisenbergstrasse 1, D-70569 Stuttgart, Germany and Institut für Theoretische und Angewandte Physik, Universität Stuttgart, D-70550 Stuttgart, Germany

J. Pflaum
3 Physikalisches Institut, Universität Stuttgart, D-70569 Stuttgart, Germany

E. Barrena and H. Dosch
Max-Planck-Institut für Metallforschung, Heisenbergstrasse 1, D-70569 Stuttgart, Germany

(Received 17 June 2003; accepted 30 October 2003)

Nanometer sized Au clusters deposited on a silicon substrate forming $Au-SiO_2-Si$ structure are important for the development of contacts in nanotechnology. Systematic x-ray reflectivity, scanning probe microscopy, and scanning tunneling spectroscopy measurements were done to understand the relationship between morphology and electrical transport properties of this nanostructural metal–insulator–semiconductor system. The presence of an interfacial layer at the metal–insulator interface dictates the tunneling current through this structure and exhibits a gap leading to a suppression of current. Local density of states and electron density/thickness of the interfacial layer have been extracted from the measurements to understand the evolution of metallicity of this $Au-SiO_2-Si$ structure. © *2004 American Institute of Physics.* [DOI: 10.1063/1.1635989]

I. INTRODUCTION

The structural and electronic properties at the interfaces of metal–insulator–semiconductor (MIS) structures have been the subject of research for decades.[1] In spite of extensive theoretical and experimental investigations on this type of system, there exist many open questions particularly when the size of the deposited metal is confined in nanometer length scale in any direction and the electrons have to travel ballistically through the metal to the metal–insulator interface. Low energy electron diffraction, Auger electron spectroscopy, and scanning tunneling microscopy (STM) and other studies seem to point to the formation of Au grains oriented along (111) planes and the presence of a disordered region around the interface.[2–4] Due to the geometrical mismatch at the Au/Si(001) interface it is difficult to compute accurate electronic properties of that region.[2] When a thin layer of SiO_2 is present on Si, the barrier formed at the metal–SiO_2 interface is much higher than that obtained directly at the metal–semiconductor contact because of the large band gap of SiO_2. Although ballistic electron emission microscopy studies have been done on the $Au/SiO_2/Si(001)$ system,[5] we are far from complete understanding of the electron transport across such interface barrier, especially for nanometer-sized Au clusters and films.

In this study, our aim is to correlate the morphology and electrical transport properties of $Au/SiO_2/Si(001)$ structure using three different experimental techniques. The electron density profile (EDP) along the depth was extracted from x-ray reflectivity measurements. Atomic force microscopy (AFM) and STM were used to observe the surface morphology. We performed current–voltage ($I-V$) measurements on this system using the scanning tunneling spectroscopy (STS) technique to obtain the local density of states (LDOS) of this system as a function of Au coverage. The influence of metal–insulator interface on the tunneling current has been explained in terms of a double barrier model.[6]

II. EXPERIMENTS

Au films were deposited on *n*-type Si(001) substrate (without removing the native oxide layer) employing a rf magnetron sputtering technique (Pfeiffer PLS500), which is extensively used for device fabrication.[7] These substrates were successively cleaned with trichloroethylene, acetone, and methanol in an ultrasonic bath prior to deposition. Four films A, B, C, and D were deposited for 10, 30, 40, and 50 s, respectively, keeping the power, Ar pressure during deposition, and base pressure fixed at 30 W, 3×10^{-3} mbar, and 4.0×10^{-6} mbar, respectively. The x-ray reflectivity measurements of these films were performed using a 18 kW rotating anode (FR 591 Enraf Nonius) x-ray source with Cu $K_{\alpha1}$ line monochromatized by a Si(111) crystal.[8] $I-V$ characteristics of the $Au-SiO_2-Si$ structure present in the films were obtained from the STS measurements at room temperature in ultrahigh vacuum (UHV) condition (Omicron Nanotechnology GmbH) using a chemically etched W tip. After etching, the tips were immersed in alcohol to avoid oxidation and they were exposed in air for 2–3 min before introducing them into the vacuum chamber. In order to be sure that the tip is not responsible for any insulating behavior

[a]Author to whom correspondence should be addressed; electronic mail: milan@lotus.saha.ernet.in
[b]Present address: Physical and Theoretical Chemistry Laboratory, South Parks Road, Oxford OX1 3QZ, UK.

observed in STS measurements, we have taken $I-V$ curves on Au(111) single crystal (shown in Fig. 5) and compared the data with the standard one. All the STM topographs were taken in constant current mode using a sample bias of -1.5 V and a set current of 0.5 nA and AFM measurements were made in contact mode using the same UHV setup.

III. RESULTS AND DISCUSSION

A. EDP from x-ray reflectivity

In x-ray reflectivity measurements, a well collimated monochromatized x-ray beam is made to incident on sample surface at a grazing angle α (starting from a few milliradians) and the reflected intensity is recorded in the plane of incidence at an angle β. In specular conditions, the incidence angle (α) and scattered angle (β) are equal ($\alpha=\beta=\theta$, say) and only the nonzero component of wave vector ($\mathbf{q}$) is given by $q_z=(4\pi/\lambda)\sin\theta$, which is perpendicular to the sample surface. Here λ is the wavelength of the x ray used. For x rays, the refractive index of any material is slightly less than unity and a positive critical angle α_c and corresponding critical wave vector q_c can be obtained. By defining wave vector in medium n as $q_{z,n}=(q_z^2-q_{c,n}^2)^{1/2}$, the reflectance at any sharp interfaces separating two media n and $n+1$, can be written as[8–10]

$$r_{n,n+1}=\frac{q_{z,n}-q_{z,n+1}}{q_{z,n}+q_{z,n+1}}. \tag{1}$$

For a thin film of thickness d (medium 1) deposited on a substrate (medium 2) the reflectance can be expressed as[8–10]

$$r(q_z)=\frac{r_{0,1}+r_{1,2}\exp(iq_{z,1}d)}{1+r_{0,1}r_{1,2}\exp(iq_{z,1}d)}, \tag{2}$$

where the air/vacuum is considered as medium 0 with the assumption that $q_z=q_{z,0}$. The measured reflected intensity $I(q_z)$ can then be written as

$$I(q_z)=I_0R(q_z). \tag{3}$$

Here I_0 is the incident intensity of x ray of wavelength λ and $|r(q_z)|^2$ is the reflectivity $R(q_z)$. For a uniform thin film $R(q_z)$ can be written using Eq. (2) as

$$R(q_z)=|r(q_z)|^2=\frac{r_{0,1}^2+r_{1,2}^2+2r_{0,1}r_{1,2}\cos(q_{z,1}d)}{1+r_{0,1}^2r_{1,2}^2+2r_{0,1}r_{1,2}\cos(q_{z,1}d)}. \tag{4}$$

It follows from Eq. (4), that the reflectivity profile $R(q_z)$ will contain[11] interference fringes, i.e., Kiessig fringes. The difference between successive minima of these fringes is inversely related to the thickness of the film d. This formalism can be generalized for a film having an EDP that can be approximated by N discrete layers each having thickness d_n and electron density ρ_n. The reflectivity of this N-layered system is calculated using a recursion relation.[8–11] The obtained profile is then fitted to the experimental reflectivity profiles to extract EDP. For a real system one has to include the effect of roughness in reflectance of each interface and Eq. (1) becomes modified as

$$r_{n-1,n}^m=r_{n-1,n}\exp(-0.5q_{(n-1)z}q_{nz}\sigma_n^2), \tag{5}$$

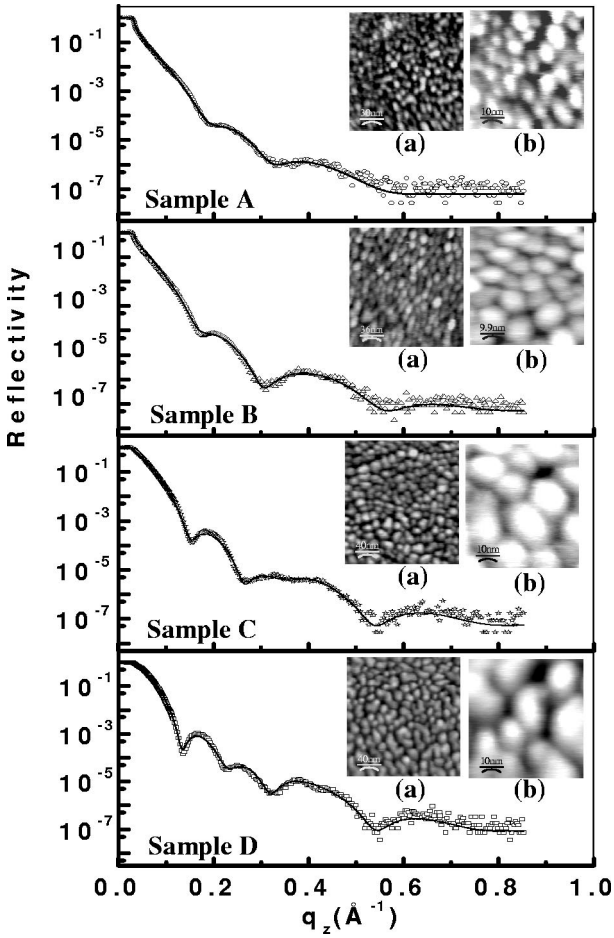

FIG. 1. X-ray reflectivity data and fitted curves (solid lines) for four samples. (Inset) Typical (a) AFM and (b) STM topographs of all samples.

where σ_n is the roughness at the interface of $(n-1)$th and nth layer. These reflectances can then be used to calculate the reflectivity $R(q_z)$ of the entire film in the above mentioned recursive formula iteratively.[8–11]

The $x-y$ average EDP as a function of depth $\rho(z)$ can be written as

$$\rho(z)=\sum_1^n \Delta\rho_i f(z_i,\sigma_i), \tag{6}$$

where $\Delta\rho_i$ is the change in electron density at ith interface located at a position z_i and f is an error function given by

$$f(z_i,\sigma_i)=f(z-z_i,\sigma_i)$$
$$=\sigma_i^{-1}(2\pi)^{-1/2}\int_{-\infty}^{z-z_1}\exp(-t^2/2\sigma_i^2)dt, \tag{7}$$

where σ_i is the roughness of the ith interface which is a parameter for the estimation of interfacial width. It can be noted that these error functions of Eq. (6) come as Debye–Waller like functions for the reflectance of each interface in reciprocal space as given in Eq. (5).

X-ray reflectivity profiles, AFM and STM images of four films A, B, C, and D are shown in Fig. 1. We divided each film into a few layers having constant electron densities for calculating the reflectivity profiles using the above men-

tioned formalism and then these profiles were fitted to the experimental data. The fit parameters were the thickness (d) and electron density (ρ) of each layer. The roughness parameters for each layer (σ) and that of the top surface and the film–substrate interface were also kept as free parameters for fitting. The roughness convoluted EDP [refer to Eq. (6)] for each film obtained by fitting the reflectivity data are shown in Fig. 3. The total thickness of A, B, C, and D films were found to be 55, 66, 73, and 81 Å, respectively, from the analysis. As seen from the EDP, the electron density attains its highest value near the top of the film, then decreases to an intermediate value in the Au–substrate interface, and finally reaches the electron density of Si through the SiO_2 layer. The maximum electron density is found to be 52%, 56.5%, 65%, and 69% of that of the bulk value of Au (4.4 electron/Å^3). Such reduction in electron density and the shapes of the EDPs of all the four films indicate island growth[12] with low surface coverage of Au on Si substrate. With an increased deposition time, as in film B, C, and D, islands grow in all directions resulting in an increase in thickness and electron density of the film. The shapes of the EDPs of all the films indicate the presence of an interfacial layer at the Au–SiO_2 interface with a lower electron density than that at the top portion of the film. The thickness and the electron density of this interfacial layer will be discussed in the following sections.

B. Bearing ratio from scanning probe microscopy (SPM)

AFM and STM images show island growth of Au on the substrate surface in each sample. The region in between two islands, which looks like a black patch in AFM and STM images, may not be the substrate surface. It is the maximum depth [denoted as h in Fig. 2(a)] beyond which AFM/STM cannot probe. In all AFM/STM height measurements this is taken as the reference zero height. Thus when we place the STM tip at a position like point A in Fig. 2(a), we do not know the actual height of this point from the substrate surface. In order to obtain the actual height of this region from the substrate surface we have to subtract the depth (h) from the total thickness (d) of the film as depicted in Fig. 2(a). To know the value of h for different films and to get an idea about the change in island shape with the increase in deposition time one can plot the average bearing ratio[12] obtained from the AFM and STM images. It is obtained by integrating the height histogram from the top surface. The bearing ratio is actually a two-dimensional (2D) projection of a 3D surface. It gives the percentage of covered area in a film at a particular height. Theoretically one can calculate the bearing ratio from simple geometry and to perform that calculation here we consider an ellipsoidal island present on a flat surface. The equation of an ellipsoid is given by

$$\frac{x^2+y^2}{a^2}+\frac{z^2}{c^2}=1,$$

where $2a$ is the axis length along x and y direction and $2c$ is the same along the z direction. The radial distance of any point from the center is given by $r=(a^2\sin^2\theta+c^2\cos^2\theta)^{1/2}$ using the parametric equation of an ellipsoid. Now the area of any slice cut from this ellipsoid [as shown in Fig. 2(b)] is given by

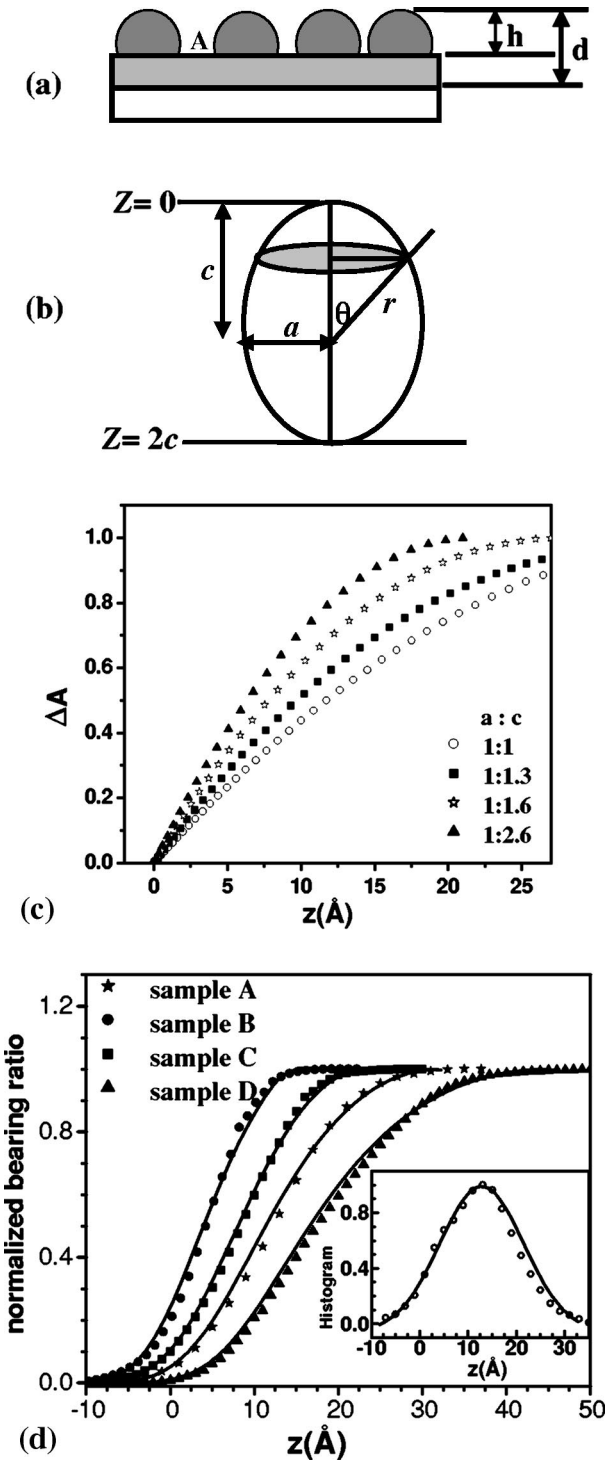

FIG. 2. (a) Schematic of a surface with islands interconnected with an interfacial layer at the bottom. SPM cannot probe beyond the depth h. (b) Area of a slice (ΔA) cut from an ellipsoidal island is shown along with geometrical parameters used in the calculation. (c) Plot of ΔA vs z for different a:c ratios. All the curves are normalized to unity. (d) Theoretical bearing ratio curves (solid lines) which matches with the experimental ones (symbols) for all four samples. For sample A, B, C, and D, the experimental bearing ratio curve matches the theoretical one for a:c=1:1.6, 1:4, 1:2.6, and 1:1.3, respectively. Inset: $d(\Delta A)/dz$ vs z plot for a:c=1:1.6 (solid line) and the height histogram (open circle) obtained from STM for sample A.

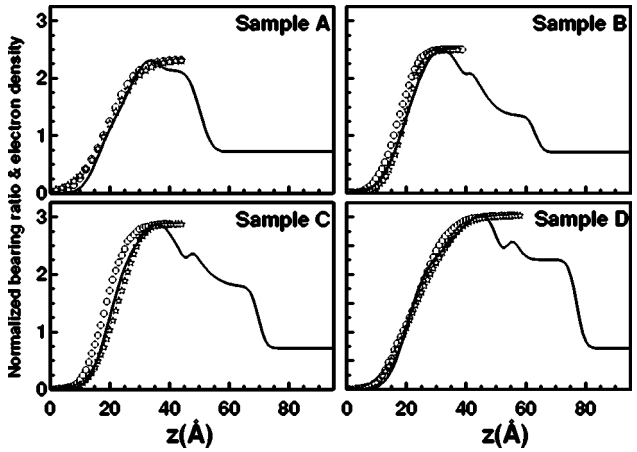

FIG. 3. EDP (solid line) obtained from x-ray reflectivity and normalized bearing ratio obtained from AFM (open circle) and STM (open star) for four samples.

$$\Delta A = \pi r^2 \sin^2\theta = \pi(a^2 \sin^2\theta + c^2 \cos^2\theta)\sin^2\theta. \quad (8)$$

The bearing ratio curve can be obtained by plotting ΔA as a function of height z where

$$z = c - r\cos\theta = c - (a^2 \sin^2\theta + c^2 \cos^2\theta)^{1/2}\cos\theta. \quad (9)$$

The differential area, $d(\Delta A)/dz$ when plotted against z will give the corresponding histogram. Figure 2(c) shows a plot of ΔA versus z for different $a:c$ ratios. It is clear from Fig. 2(c) that the rising slopes of the curves are different for different $a:c$ ratios. These theoretical curves are then fitted to the experimental ones. Before the fitting, we convoluted the theoretical curves with a Gaussian of full width at half maximum ~5 Å which takes care of the effect of tip apex as well as the overall roughness of the film since the experimental bearing ratio curve gives the average information over a certain region.

The experimental bearing ratio curves obtained from STM images for all four samples are shown in Fig. 2(d). In our case the plotted bearing ratio is the average of a number of bearing ratios calculated for different images taken at different locations on a sample. The difference in rising slopes of the curves can be attributed to different shapes of islands for different films. For films A, B, C, and D, the experimental bearing ratio curves match with the theoretical ones for $a:c = 1:1.6$, 1:4, 1:2.6, and 1:1.3, respectively, and their derivatives give the corresponding height histograms as shown for sample A in the inset of Fig. 2(d). We shall discuss the shapes of islands in different films in more detail after comparing the bearing ratio curve with the EDP in the next section.

C. Comparison of bearing ratio with EDP

In Fig. 3 we plotted average bearing ratio curves obtained from AFM and STM images along with the EDP obtained from the x ray. Here the plotted bearing ratio was normalized to the maximum of EDP. It is interesting to note that we observed a similar nature of profiles obtained from real and reciprocal space measurements, indicating the presence of a particular shape and size of the islands. The effect of local roughness, which gets convoluted with the island shape in EDP, can be neglected here as from STM/AFM measurements this value was found to be less than 2 Å. For samples A, B, C, and D, from the bearing ratio plot we can get information up to the depth (h) of 44, 40, 44, and 51 Å respectively. Now for sample A the average island radius a ~27 Å as obtained from the STM image. Then $a:c = 1:1.6$ gives $c \sim 43$ Å which is very close to h (44 Å) as obtained from Fig. 3. That means, for sample A, the top half portion of the ellipsoidal island (that is accessible to AFM and STM measurements) is contributing to the bearing ratio. Now subtracting h from total thickness d obtained from EDP we get the thickness of the interfacial layer as 11 Å. The schematic of the film will look like Fig. 2(a). Similarly for sample B, $a \sim 50$ Å, $a:c = 1:4$, and $c \sim 200$ Å. But here h is obtained as 40 Å. That means in this sample the entire top half portion of the island is not contributing to the bearing ratio as in the case of sample A. Here only the top 40 Å, which is 20% of c, is responsible for the steep rise in the bearing ratio curve. For this sample, subtracting h from d, we find the thickness of the interfacial layer as 26 Å. We have tabulated all these parameters for four samples in Table I.

TABLE I. Parameters obtained by comparing bearing ratio with EDP for four samples.

Sample	a (Å)	$a:c$	c (Å)	h (Å)	% of c contributing in bearing ratio	d (Å) from x ray	$d-h$ (Å)
A	27	1:1.6	43	44	100	55	11
B	50	1:4	200	40	20	66	26
C	70	1:2.6	182	44	24	73	29
D	75	1:1.3	97.5	51	52	81	30

The above results indicate that the islands present in all the films are prolate spheroidal ($c > a$) in shape and the bottom parts of the islands are interconnected with an interfacial layer. As deposition time increases from sample A to B, the c/a value suddenly increases from 1.6 to 4.0, indicating columnar growth in sample B. With more increase in deposition time the columnar islands start to flatten, leading to a decrease in c/a value (refer to Table I). The thickness of the interfacial layer gradually increases from sample A to D. From the above calculations we get the thickness of the interfacial layer, which is basically the actual height of the region in between islands, as 11, 26, 29, and 30 Å for films A, B, C, and D, respectively. Therefore when we place the STM tip in between islands during STS, we are getting information from the interfacial layer, not from the substrate surface. The average electron density of the interfacial layer (refer to Fig. 3) comes out to be 1.3, 1.7, 2.0, and 2.3 electron/Å^3 for films A, B, C, and D, respectively. At this stage it is difficult to specify the actual composition and structure of this interfacial layer, but it has to be a network of Si–O–Au that is generating the in between electron densities. We plan to carry out further SPM studies by depositing these films within the SPM vacuum chamber.

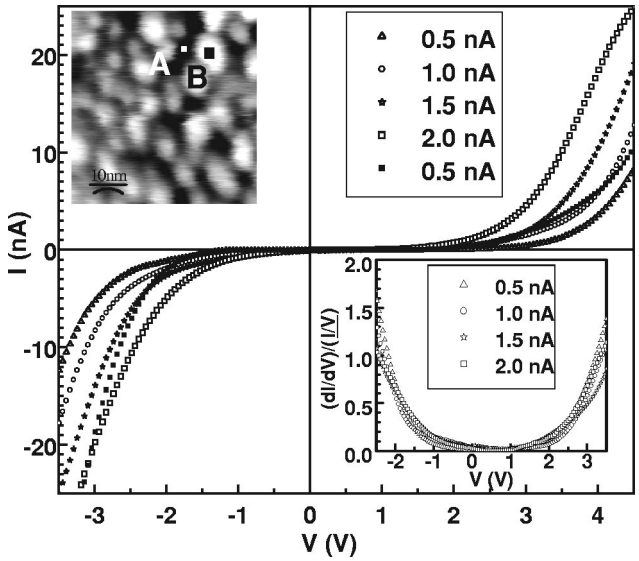

FIG. 4. $I-V$ curves for different set currents with initial sample bias of -1.5 V taken on A and B positions of sample A (as shown in the STM image at the top left inset). Open symbols denote $I-V$ curves for different set currents obtained at A. Closed symbols denote the $I-V$ curve at point B. Bottom right inset: $(dI/dV)/(\underline{I/V})$ vs V plots for different set currents obtained at point A.

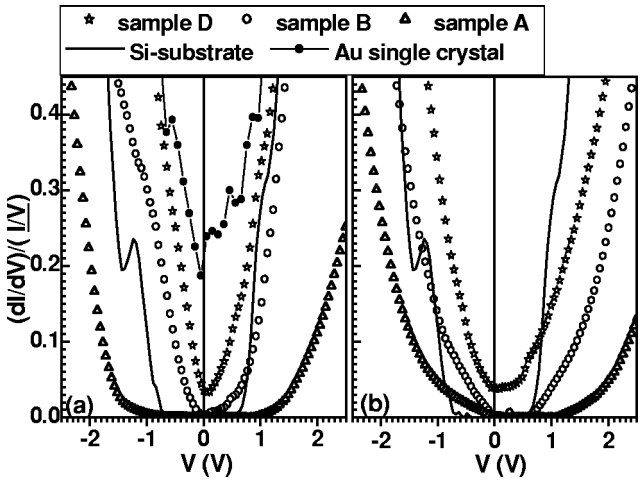

FIG. 5. $(dI/dV)/(\underline{I/V})$ vs V plots obtained (a) on islands and (b) in between islands for different samples. The Au(111) single crystal data is reduced five times to fit in the scale.

D. STS measurements

We performed systematic STS measurements of all the four films by placing the STM tip above chosen positions on islands and in between the islands. Each curve was recorded by keeping the feedback loop off and in each case four $I-V$ curves were taken at four different tip–sample separations by changing the set current. The $I-V$ curves thus obtained on different islands of each sample have similar nature, i.e., they all have the same slope and a suppression of current is observed around zero bias. In Fig. 4 we have shown a STM image of sample A and $I-V$ curves taken on an island (marked B) and in between islands (marked A) for different set currents, as examples. The $I-V$ curves obtained inbetween islands are different in nature. All the $I-V$ curves shown in this article are representative of 10–15 curves taken at different locations of the sample and each curve is highly reproducible. When we plot normalized $(dI/dV)/(I/V)$ curves as a function of bias voltage, which is a direct measure of LDOS,[13] the dependence of current on tip–sample separation is removed and four curves merge as shown in the case of sample A (Fig. 4). The threshold voltage V_{th} (determined with an accuracy of 0.1 eV), after which the current starts to increase are shown in Fig. 5 for different samples. Following Bardeen's transfer Hamiltonian approach[14] we can explain our observations with the assumption that the DOS of the W tip is constant over the range of measurements. Accordingly

$$\frac{dI}{dV} \propto \rho_s(\mathbf{r}, E_F - eV), \tag{10}$$

where $\rho_s(\mathbf{r}, E_F - eV)$ is the local density of states of the sample evaluated at the tip position[15] $\mathbf{r}=(x,y,z)$ and at energy $E=E_F-eV$. Thus in our measurement we are probing the LDOS of a MIS system. In the case of tunneling through a MIS system the voltage threshold for tunneling should be half of the semiconductor band gap if the Fermi level lies at the midgap. The symmetric nature of $V_{\text{th}}=\pm 0.6$ V for *n*-type Si(001) used here as bare substrate, where the Fermi level should move towards the conduction band by 0.3 eV depending on the concentration of the dopant in the substrate, arises due to band bending. Larger threshold value $V_{\text{th}}=\pm 0.9$ V observed on islands of sample A as compared to the substrate can be explained by considering a double barrier tunneling model where the electrons have to travel through two barriers: one formed by insulating SiO_2 layer in between Si and Au film and the other formed by vacuum in between Au film and the STM tip. The Au film that is present inbetween two barriers is made of two portions, namely, the top Au islands and the interfacial layer at the metal–insulator interface region. If we consider the band gaps of the substrate and the interfacial layer as $2E_g$ and $2E_g'$, respectively, then the observed V_{th} should be equal[16] to E_g+2E_g', which gives $2E_g'=0.3$ eV. The size of the Au island which can open up a gap of 0.3 eV can be estimated by considering a simple model of a particle in a box for independent electrons. The mean spacing of energy levels can be obtained by $\delta E = 2\pi^2\hbar^2/(m_e k_F V)$, where m_e is the electron mass, k_F is the Fermi wave vector, and V is the Au island size.[17] The level spacing is expected to be $\sim$0.3 eV for a spherical island of radius 4.6 Å which is much smaller than the islands present in our film. For these STS measurements the electrical connections were taken from the tip and from the bottom of the silicon. Therefore the electrons have to travel through a path consisting of Si–SiO_2(barrier)–interfacial layer–Au island–vacuum(barrier)–tip. If we map it to an equivalent circuit, it is clear that the Au island and the interfacial layer are in series connection with respect to the tunneling current. We further assume that the top-to-central portion of the metallic island in the path of the electron is equivalent to a lead connection in the circuit and it is not responsible for the suppression of current around zero bias. Thus in our case, it is not the whole island, but the interfacial layer of thickness $\sim$11 Å at the Au–SiO_2 interface that has opened up a gap of

0.3 eV. This phenomenon is found to be reproducible. As the thickness of the interfacial layer increases in samples B, C, and D, in the case of tunneling through these islands observed threshold voltages become equal or less than that observed for the substrate (solid line in Fig. 5). In these cases metal induced gap states are present in the substrate band gap region which are composed of the states from the tails of the metallic wave function decaying into the semiconductor side, as observed earlier.[18–20] Thus we get metallic characteristics, i.e., states at the Fermi level and conductance increases with the increase of thickness of interfacial layer from samples A to D.

When we measure tunneling currents in between islands, only the interfacial layer is present between the two barriers and this interfacial layer is exposed because of the absence of the covering islands. We assume here that due to this exposure, additional surface states are produced in the gap region. If the valence band edge of Si bends in such a way that it touches the Fermi level then the electron flows from the substrate through these surface states present in the interface gap immediately after a negative sample bias is applied,[1] resulting in a slow increase of current from 0 V for negative sample bias. Above a certain voltage tunneling occurs from the valence band states of the substrate through the conduction band states of the interfacial layer resulting in a rapid increase in current. On the other hand, for positive sample bias, current cannot flow from the tip through the surface states present in the interface gap because of unavailability of states in the band gap region of the substrate. A threshold voltage of 1.2 V is required to flow the current in this direction as shown in Fig. 5(b). It will be interesting to develop detailed calculation to quantify the asymmetric response presented here. For all other samples, with increasing Au thickness and coverage, the current increases in similar fashion when we are probing between islands.

IV. SUMMARY

We have shown using SPM and reflectivity measurement that the metal–insulator interface present in the $Au/SiO_2/Si(001)$ system determines the voltage threshold for tunneling through this MIS structure. In sample A, ellipsoidal islands are present with an interfacial layer of thickness 11 Å connecting them at the bottom. A voltage of ± 0.9 V is required to start the tunneling through these islands. This is more than the voltage threshold for tunneling through the bare substrate. This phenomenon is explained by considering a gap of 0.3 eV opened up by the interface. As the thickness of the interfacial layer increases, the $I-V$ curves start to show metallic behavior. Further structural and spectroscopic studies are required to understand the exact nature of this interface region, which can be the basis of formation of quantum well structures in metallic systems.[21]

In conclusion we have demonstrated that by combining x-ray reflectivity, STM, and AFM techniques one can extract morphology of ultrathin films, where the effect of confinement depends strongly on the morphology.[9,18] We have shown that measured STS data could be, at least qualitatively, correlated to the morphology of the films. We are planning to perform *in situ* low temperature STS measurements during Au deposition on Si(001) with and without the presence of the native oxide layer to elucidate the effect of interfacial layer further. The presented technique will also be useful for the analysis of morphology of islands in various other nanostructural systems.

ACKNOWLEDGMENT

The authors would like to thank Dr. Volker Kruppa for his technical assistance during SPM measurements.

[1] S. M. Sze, *Physics of Semiconductor Devices* (Wiley, New York, 1969).
[2] P. F. de Pablos, F. J. Garcia-Vidal, F. Flores, and P. L. de Andres, Phys. Rev. B **66**, 075411 (2002).
[3] K. Oura and T. Hanawa, Surf. Sci. **82**, 202 (1979).
[4] A. K. Green and E. Bauer, J. Appl. Phys. **47**, 1284 (1976).
[5] L. Quattropani, I. Maggio-Aprile, P. Niedermann, and Øystein Fischer, Phys. Rev. B **57**, 6623 (1998).
[6] S. Datta, *Electronic Transport in Mesoscopic Systems* (Chambridge University Press, Cambridge, 1995).
[7] F. J. Himpsel, J. E. Ortega, G. J. Mankey, and R. F. Willis, Adv. Phys. **47**, 511 (1998).
[8] J. K. Basu and M. K. Sanyal, Phys. Rep. **363**, 1 (2002).
[9] M. K. Sanyal, A. Datta, and S. Hazra, Pure Appl. Chem. **74**, 1553 (2002).
[10] V. Holy, U. Pietsch, and T. Baumbach, *X-Ray Scattering from Thin Films and Multilayers* (Springer, New York, 1999); M. Tolan, *X-Ray Scattering from Soft Matter Thin Films* (Springer, New York, 1999); J. Daillant and A. Gibaud, *X-Ray and Neutron Reflectivity: Principles and Applications* (Springer, New York, 1999).
[11] A. Gibaud and S. Hazra, Curr. Sci. **78**, 1467 (2000).
[12] S. Kundu, S. Hazra, S. Banerjee, M. K. Sanyal, S. K. Mandal, S. Chaudhuri, and A. K. Pal, J. Phys. D **31**, L73 (1998).
[13] J. A. Stroscio and R. M. Feenstra, in *Scanning Tunneling Microscopy*, edited by J. A. Stroscio and W. J. Kaiser, Methods of Experimental Physics, Vol 27 (Academic, New York, 1993), p. 95.
[14] J. Bardeen, Phys. Rev. Lett. **6**, 57 (1961).
[15] J. Tersoff and D. R. Hamann, Phys. Rev. B **31**, 805 (1985).
[16] J. C. Chen, *Introduction to Scanning Tunneling Microscopy* (Oxford University Press, New York, 1993).
[17] B. Wang, H. Wang, H. Li, C. Zeng, and J. G. Hou, Phys. Rev. B **63**, 035403 (2000).
[18] P. Moriarty, Rep. Prog. Phys. **64**, 297 (2001).
[19] P. N. First, J. A. Stroscio, R. A. Dragoset, D. T. Pierce, and R. J. Celotta, Phys. Rev. Lett. **63**, 1416 (1989).
[20] R. M. Feenstra and P. Martensson, Phys. Rev. Lett. **61**, 447 (1988).
[21] M. Milun, P. Pervan, and D. P. Woodruff, Rep. Prog. Phys. **65**, 99 (2002).